Protein Engineering, Design & Selection, 2015, vol. 28 no. 10, pp. 351–363
doi: 10.1093/protein/gzv032
Advance Access Publication Date: 4 August 2015
Original Article

Original Article

An efficient protocol towards site-specifically clickable nanobodies in high yield: cytoplasmic expression in *Escherichia coli* combined with intein-mediated protein ligation

Duy Tien Ta[1,2], Erik Steen Redeker[3], Brecht Billen[1], Gunter Reekmans[4], Josephine Sikulu[1], Jean-Paul Noben[5], Wanda Guedens[1], and Peter Adriaensens[1,4,*]

[1]Biomolecule Design Group, Institute for Materials Research (IMO), Hasselt University, Agoralaan-Building D, Diepenbeek BE-3590, Belgium, [2]Faculty of Food Technology and Biotechnology, Can Tho University of Technology, Can Tho, Vietnam, [3]Maastricht Science Programme, Maastricht University, Maastricht 6200 MD, The Netherlands, [4]Applied and Analytical Chemistry, Institute for Materials Research (IMO), Hasselt University, Agoralaan-Building D, Diepenbeek BE-3590, Belgium, and [5]Biomedical Research Institute (Biomed) and School of Life Sciences, Transnationale Universiteit Limburg, Hasselt University, Agoralaan-Building C, Diepenbeek BE-3590, Belgium

*To whom correspondence should be addressed. E-mail: peter.adriaensens@uhasselt.be
Edited by Laurent Jespers

Received 9 February 2015; Revised 28 June 2015; Accepted 1 July 2015

Abstract

In this study, several expression strategies were investigated in order to develop a generic, highly productive and efficient protocol to produce nanobodies modified with a clickable alkyne function at their C-terminus via the intein-mediated protein ligation (IPL) technique. Hereto, the nanobody targeting the vascular cell adhesion molecule 1 (NbVCAM1) was used as a workhorse. The highlights of the protocol can be ascribed to a cytoplasmic expression of the nanobody–intein–chitin-binding domain fusion protein in the *Escherichia coli* SHuffle® T7 cells with a C-terminal extension, i.e. LEY, EFLEY or His_6 spacer peptide, in the commonly used Luria-Bertani medium. The combination of these factors led to a high yield (up to 22 mg/l of culture) and nearly complete alkynation efficiency of the C-terminally modified nanobody via IPL. This yield can even be improved to ~45 mg/l in the EnPresso® growth system but this method is more expensive and time-consuming. The resulting alkynated nanobodies retained excellent binding capacity towards the recombinant human VCAM1. The presented protocol benefits from time- and cost-effectiveness, which allows a feasible production up-scaling of generic alkynated nanobodies. The production of high quantities of site-specifically modified nanobodies paves the way to new biosurface applications that demand for a homogeneously oriented nanobody coupling. Prospectively, the alkynated nanobodies can be covalently coupled to a multitude of azide-containing counterparts, e.g. contrast labeling agents, particles or surfaces for numerous innovative applications.

Key words: bioorthogonal chemistry, CuAAC, cytoplasmic expression, intein-mediated protein ligation, VCAM1-targeting nanobody

Introduction

During the past decades, technologies for controlled protein modification have remarkably evolved hand in hand with the growth of synthetic and chemical biology. Several studies have recently reported on the incorporation of bioorthogonal functional groups (i.e. not naturally present in the host organisms) in a protein of interest (Reulen *et al.*, 2009; Hao *et al.*, 2011; Heal *et al.*, 2011; Lang *et al.*, 2012; Debets *et al.*, 2013a,b; Schneider *et al.*, 2013; Choi *et al.*, 2014; Herner *et al.*, 2014). Moreover, bioorthogonal chemistry currently attracts a lot of attention for facilitating site-specific protein modifications which enable uniformly oriented protein couplings to various complementary functionalized molecules (e.g. for imaging contrast or drug release) (Hao *et al.*, 2011; Heal *et al.*, 2011; Lang *et al.*, 2012; Debets *et al.*, 2013a,b; Naganathan *et al.*, 2013; Zeglis *et al.*, 2013; Dean and Palmer, 2014; Dennler *et al.*, 2014; Hapuarachchige *et al.*, 2014; van Vught *et al.*, 2014) or material surfaces (Debets *et al.*, 2013a,b; Steen Redeker *et al.*, 2013; Trilling *et al.*, 2014) by means of highly selective chemistries (Best, 2009; Choi *et al.*, 2014).

In the area of advanced biomaterials for early disease diagnosis and therapy follow-up, antibodies are the most concerned biomolecules for targeting and biosensing purposes (Nguyen *et al.*, 2012). Recently, nanobodies have emerged as powerful next-generation antibodies for therapeutic applications (Muyldermans *et al.*, 2009). These proteins, derived from the variable domain of the heavy chain of the camelid single-domain antibody (called VHH), are much smaller and more stable than conventional full-length antibodies but retain equivalent antigen-binding capacity (Muyldermans *et al.*, 1994). Nanobodies are genetically encoded by a single gene and can thus be easily engineered and functionally expressed in *Escherichia coli* (Dumoulin *et al.*, 2002) as the smallest known antigen-binding entities (Arbabi-Ghahroudi *et al.*, 2005; Muyldermans *et al.*, 2009; Bell *et al.*, 2010; Saerens, 2010; Baral and Arbabi-Ghahroudi, 2012). These characteristics make nanobodies potential candidates for biosensor development (Hassanzadeh-Ghassabeh *et al.*, 2013) or molecular imaging purposes (Chakravarty *et al.*, 2014). In order to increase the sensitivity and/or selectivity of these biomaterials, the nanobody can be site-specifically appended with a bioorthogonal functionality, which facilitates a uniformly oriented coupling process (Steen Redeker *et al.*, 2013). Crystal structures of nanobodies show that engineering the N-terminus might influence the antigen binding since it is positioned close to the complementarity determining regions (CDRs) (Kijanka *et al.*, 2015) which essentially contribute to binding activity (De Genst *et al.*, 2006; Muyldermans *et al.*, 2009; Broisat *et al.*, 2012). Therefore, site-specific modification is targeted at the nanobody's C-terminus which is spatially positioned on the opposite side. Various techniques have been developed for this purpose, among which is the intein-mediated protein ligation (IPL) (Ghosh *et al.*, 2011). This technique, also called expressed protein ligation, was first described by Muir and coworkers to ligate a phosphotyrosine-containing peptide or an unnatural amino acid to the C-terminus of recombinant proteins (Muir *et al.*, 1998; Ayers *et al.*, 1999). In IPL, a protein of interest is fused to a self-cleavable peptide sequence called intein (or protein intron), which catalyzes an N-S shift at the protein's terminus to form a thioester intermediate. This is subsequently subjected to a nucleophilic attack and ligation with a thiol-containing molecule-like dithiothreitol (DTT) via a process called native chemical ligation (Dawson *et al.*, 1994; Muir *et al.*, 1997) (Scheme 1, left). The DTT molecule can then be removed from the target by hydrolysis to finally generate the wild-type protein, thus promoting a single-step purification of the protein of interest (Chong *et al.*, 1997). The nucleophile can also be a bifunctional molecule, e.g. a cysteine-alkyne linker that carries both a thiol group and a bioorthogonal alkyne group (Scheme 1, right) (Lin *et al.*, 2006). To improve the modification efficiency, 2-mercaptoethanesulfonic acid (or MESNA, Supplementary Fig. S1A) is usually added as the primary nucleophile to produce the thioester intermediate, which then undergoes a second nucleophilic attack by the cysteine-alkyne linker (Xu and Evans, 2001). In this way, the linker molecule becomes covalently bonded to the protein's terminus, leaving the alkyne moiety available to selectively react with an azide-containing molecule in a 'click' reaction, e.g. the copper (I)-catalyzed Huisgen 1,3-dipolar azide-alkyne cycloaddition (CuAAC) (Tornoe *et al.*, 2002; Meldal and Tornoe, 2008) or the strain-promoted alkyne-azide cycloaddition (Debets *et al.*, 2011).

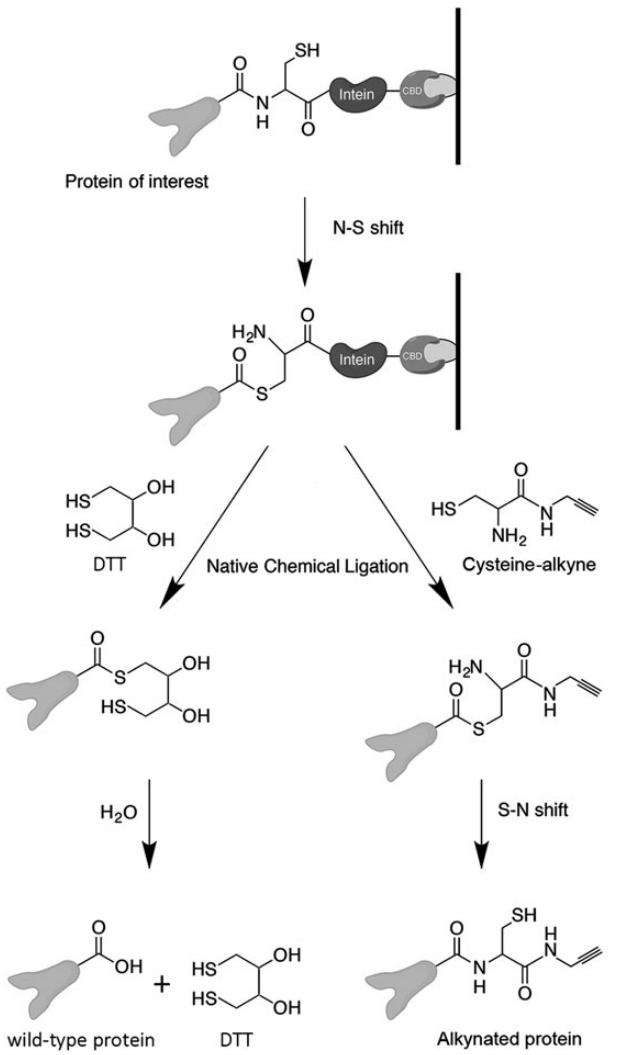

Scheme 1. The IPL mechanism (picture adapted from Steen Redeker *et al.* (2013)). The gene encoding the protein of interest is C-terminally fused to an intein–CBD. The expressed fusion protein is purified by affinity chromatography on a chitin column. On-column cleavage of the target protein from the intein is performed by adding a thiol nucleophile, e.g. DTT or a cysteine-alkyne linker. Whereas DTT—after subsequent removal by hydrolysis—results in the wild-type protein (bottom left), the cysteine-alkyne linker results in the attachment of a bioorthogonal alkyne function to the C-terminus of the released protein (bottom right).

The IPL technique using DTT as the nucleophile has been intensively applied for protein purification (Warren *et al.*, 2013; Luan *et al.*, 2014; Wood and Camarero, 2014). IPL-mediated protein modification has also been investigated for several other applications, for example, to functionalize enhanced Green Fluorescent Protein and aldo-keto reductase with a fluorescent dye or covalently couple them to polyethylene glycol resins (Steinhagen *et al.*, 2011), to cyclize the cysteine-rich wheat metallothionein for stability enhancement (Tarasava and Freisinger, 2014) or to produce the human islet amyloid polypeptide at considerable yield in *E.coli* (Rodriguez Camargo *et al.*, 2015). Site-specific conjugation of an alkyne-containing murine dihydrofolate reductase with an azido-containing biotin derivative is recently achieved using CuAAC and the resulting enzyme retained a high catalytic activity (Lim *et al.*, 2014). This is in contrast to commonly used non-site-specific protein coupling methods which frequently lead to protein-conjugated materials with low performance as not all active sites are accessible anymore for the target analytes. Despite that many studies describe the use of IPL techniques for different proteins, there is today only a limited number of reports regarding the combined use of IPL and 'click' chemistry on diagnostic or therapeutic nanobodies to create functionalized materials, e.g. using the nanobody against glutathione S-transferase (sdAb-aGST) for micelles synthesis (Reulen *et al.*, 2009) and PlexinD1 for polymersomes with tumor-targeting potential (Debets *et al.*, 2013a,b). However, these nanobodies were produced in rather low yields. This explains the general need for a protocol which leads to a significant improvement of the yield and modification efficiency of site-specifically clickable nanobodies in order to make up-scaling and subsequent exploration of innovative applications feasible.

In the present study, we employed the nanobody targeting the vascular cell adhesion molecule-1 (NbVCAM1). NbVCAM1 is a promising candidate for diagnostic and/or therapeutic purposes since VCAM1 plays an important role in the recruitment of leukocytes to the endothelium during atherosclerosis (O'Brien *et al.*, 1993), as well as being a potential marker for certain types of cancer (Shioi *et al.*, 2006; Touvier *et al.*, 2012). Different strategies for engineering and expression of NbVCAM1 were explored in order to achieve high yields and alkynation efficiencies. The nanobody was expressed as a fusion protein with the intein and chitin-binding domain (CBD), which was then subjected to *in vitro* IPL-mediated alkynation.

Nanobody expression is usually performed in the periplasm of *E.coli* to facilitate proper protein folding in the oxidizing periplasmic space. Periplasmically expressed proteins are less susceptible to proteolysis and require simpler down-stream purification processes. This method requires an N-terminal signal peptide (leader sequence) to facilitate protein transport to the periplasm via the bacterial secretory machinery. This, however, not always ensures an efficient translocation of heterologous proteins (Makrides, 1996) and can lead to partially processed proteins and truncated leader sequences (Reulen *et al.*, 2009). On the other hand, cytoplasmic expression often requires a cumbersome refolding step due to the reducing cytosolic environment that might harm the intradomain disulfide bonds (Harmsen and De Haard, 2007; de Marco, 2012). However, cytoplasmic expression of functional nanobodies has been reported by Zarschler *et al.* (2013) using the SHuffle® T7 *E.coli* strain. This strain constitutively expresses a chromosomal copy of the DsbC chaperone, which exhibits disulfide bond isomerase activity to correct mis-oxidized disulfide bonds (Bessette *et al.*, 1999; Chen *et al.*, 1999; Levy *et al.*, 2001). Therefore, the NbVCAM1 gene was engineered for both periplasmic and cytoplasmic expression, i.e. with and without an N-terminal *pelB* leader sequence, respectively. Several studies have employed the N-terminal *pelB* sequence specifically for expression of different types of antibodies in *E.coli* to avoid the formation of inclusion bodies (Corisdeo and Wang, 2004; Reulen *et al.*, 2009; Ghassabeh *et al.*, 2010; Hassanzadeh-Ghassabeh *et al.*, 2011). Since tyrosine and histidine residues are described as the most optimal for intein cleavage (Xu and Evans, 2001), the nanobody's C-terminus was further engineered with one of the following three spacer peptides between the nanobody and the intein—EFLEY, LEY or His_6-tag—to enhance independent folding of the nanobody and the intein–CBD domain, and to enhance the efficiency of the IPL process. Last but not least, the expression is compared with two *E.coli* strains, i.e. the conventional BL21(*DE3*) and the SHuffle® T7, as well as in three different growth media: Luria-Bertani (LB), terrific broth (TB) and EnPresso®. The optimized protocol allows a high-yield expression of nanobodies and nearly complete degree of (site-specific) alkynation. The proposed protocol to efficiently synthesize C-terminally alkynated nanobodies is a major step forward when compared with the current state-of-the-art, and can be translated to other nanobodies due to their conserved structures, as mentioned before. It opens the way towards new applications such as nanobody-fluorescent contrast conjugates, nanobody-nanoparticle drug carriers and nanobody-based biosensors.

Materials and methods

Materials

Unless stated below, all chemicals and reagents were obtained from Sigma. The primers (Supplementary Table SI) were ordered from Eurogentec. The PCR reagents, restriction enzymes and B-PER reagent were purchased from Thermo Scientific. The pHEN6(c) and pHEN6(a) plasmids containing the NbVCAM1-His_6 and NbBcII-10-His_6 (nanobody targeting the bacterial β-lactamase) genes were kindly provided by Prof. Serge Muyldermans (Vrije Universiteit Brussel). The pTXB1 and pMXB10 vector, *E.coli* BL21(*DE3*) and SHuffle® T7 competent cells, B-PER reagent and chitin resin were purchased from New England Biolabs. The EnPresso® growth system package was bought from BioSilta. The BCA protein assay kit was purchased from Thermo Scientific. The recombinant human VCAM1/CD106 Fc Chimera (containing a human VCAM1 domain, a human IgG domain and a C-terminal His_6-tag) was bought from R&D Systems. The cysteine-alkyne linker (2-amino-3-mercapto-*N*-(prop-2-ynyl) propionamide) was purchased from AnaSpec. The azido-biotin derivative (Supplementary Fig. S1B) was synthesized from 1-bromo-3-aminopropane and the NHS-ester of biotin (Sigma). Briefly, the 1-bromo-3-aminopropane was azidified to form 1-azido-3-aminopropane according to Carboni *et al.* (1993) which was then coupled to biotin via NHS-coupling, resulting in the azido-biotin.

Methods

Molecular cloning of the nanobodies

A schematic description for cloning and expression of all nanobody variants explored in this study is shown in Fig. 1. The NbVCAM1 gene was amplified from the plasmid pHEN6(c):*pelB*-NbVCAM1-His_6 (Broisat *et al.*, 2012) (construct **1**) using different pairs of primers (Supplementary Table SI) for the different expression strategies. The BIO125 forward primer is designed to comprise the *pelB* leader sequence in order to facilitate periplasmic translocation, while BIO126 does not and is used for cytoplasmic expression. The reverse primers contain sequences encoding for different spacer peptides. All PCRs were run at 95°C for 5 min, followed by 30 cycles of 95°C for 30 s, 55°C for 30 s and 72°C for 45 s. A final elongation step of

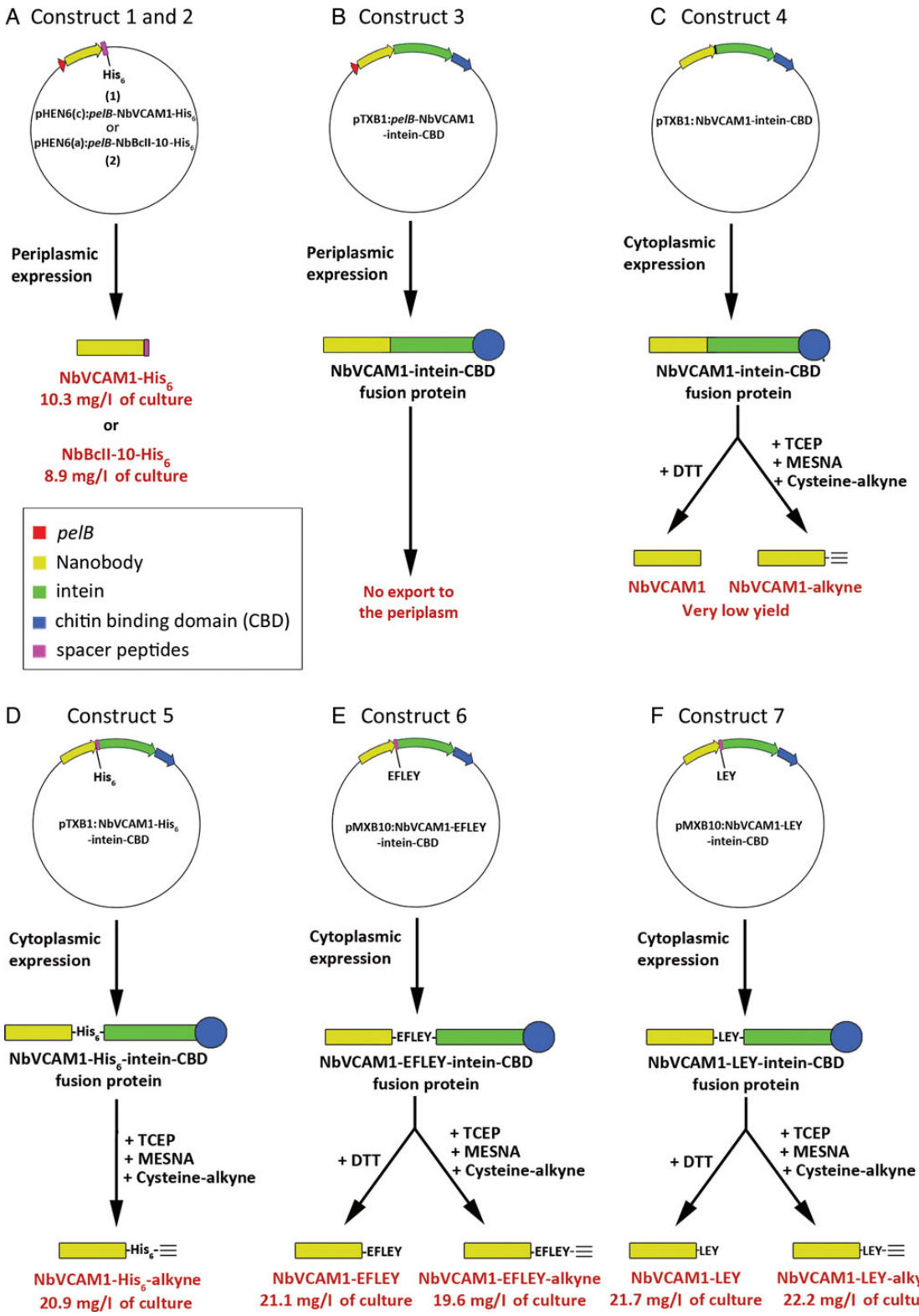

Fig. 1 Schematic description of the cloning and expression of the different nanobody variants. The IPL-mediated production strategy of unmodified and alkynated nanobodies is shown and their corresponding yields are displayed at the bottom.

10 min at 72°C was performed, followed by holding at 4°C. The PCR products were cloned into either the pTXB1 or the pMXB10 vector, making use of the appropriate restriction sites for the different expression strategies of choice (Supplementary Table SII). For the pTXB1 vector, cloning of the NbVCAM1 gene (with or without *pelB*—amplified by the BIO125 or BIO126 forward primer,

respectively, and the reverse primer BIO123) by using the NdeI and SapI restriction sites resulted in the in-frame fusion of the nanobody with the intein and CBD sequences, without any extra residues between the nanobody and the intein (constructs **3** and **4**). However, using the BIO175 reverse prime including the His_6-tag-encoding sequence resulted in the addition of a His_6-tag spacer peptide between the nanobody and the intein (construct **5**). For the addition of the other spacer peptides, the pMXB10 vector was digested using either NdeI/EcoRI or NdeI/XhoI. This removes the sequence encoding the maltose binding protein (MBP) from the original vector, but leaves a small residual sequence encoding the EFLEY or LEY spacer peptide, respectively, at the 5′-end of the intein sequence. These sequences were then fused in-frame with the nanobody gene (without *pelB*), resulting in either the EFLEY (construct **6**) or LEY (construct **7**) spacer peptide between the nanobody and the intein. All constructs were confirmed by sequencing.

Optimization of the nanobody–intein–CBD fusion protein expression

To determine the optimal isopropyl β-D-1-thiogalactopyranoside (IPTG) concentration and temperature for periplasmic and cytoplasmic nanobody expression in LB medium, constructs **3** and **4** were transformed into *E.coli* BL21(*DE3*) and small scale expressions were performed under different culture conditions. A fresh single colony was selected and pre-cultured in 3 ml LB supplemented with 100 µg/ml Ampicillin (LB^{Amp}) at 37°C overnight while shaking. A secondary culture of 50 ml LB^{Amp} was made by inoculation 1/100 with the pre-culture. This culture was grown at 37°C while shaking until the OD_{600} reached 0.5. Protein expression was then induced by adding IPTG at a final concentration of 0, 0.5 or 1 mM. The cells containing construct **3** were grown further overnight at 18 or 28°C since low temperature and long expression time are necessary for efficient periplasmic translocation (Makrides, 1996; Rosano and Ceccarelli, 2014), whereas the cells containing construct **4** were grown further for 3 h at 28 or 37°C. Subsequently, the cells were harvested by centrifuging at 5 000 *g* for 10 min, suspended in 2× Laemmli sample buffer, boiled for 5 min and analyzed for total cell protein (TCP) content on a 12% SDS–PAGE gel. The experimental conditions which led to the highest amount of the fusion protein (determined via SDS–PAGE) were used to perform a large-scale protein expression.

Upscaled expressions using the *E.coli* BL21(DE3) in LB medium and protein extraction

In order to compare the influence of the spacer peptides on the IPL-mediated alkynation efficiency, cells containing constructs **3–7** were cultured and induced in a volume of 300 ml LB^{Amp} using the optimized conditions for IPTG concentration, post-induction temperature and time (for periplasmic expression: 0.5 mM IPTG, 18°C, overnight; for cytoplasmic expression: 0.5 mM IPTG, 37°C, 3 h). Periplasmic extraction was performed using an osmotic shock protocol as described by Saerens *et al.* (2004), while cytoplasmic extraction was done by re-suspending the cells (of a 300 ml culture) in 6 ml B-PER reagent (supplemented with 6 units of DNaseI) and incubating at room temperature for 15 min. Clear cell lysates from both extractions were obtained by centrifuging at 20 000 *g* for 30 min at 4°C. The TCP content before and after IPTG induction, as well as the cell lysate and the cell debris were analyzed on a 15% SDS–PAGE gel. In addition, the expression and purification of the His_6-tagged nanobodies: NbVCAM1-His_6 (construct **1**) and NbBcII-10-His_6 (construct **2**) were carried out as described by Saerens *et al.* (2004). These nanobodies were used as controls in the ELISA tests.

IPL-mediated alkynation

The clear cell lysates from cells expressing constructs **4–7** were loaded on 5 ml, 5 mm diameter columns packed with 1.5 ml chitin resin, pre-equilibrated with column buffer (CB) (20 mM HEPES, 500 mM NaCl and 1 mM EDTA at pH 8.5). The columns were thoroughly washed with 20 bed volumes of CB. Cleavage of the nanobody from the intein was done by quickly flushing each column with 1.5–2 bed volumes and then filling with 1 bed volume of (i) pure CB as control, (ii) CB containing 30 mM DTT or (iii) CB containing 1 mM cysteine-alkyne linker supplemented with 30 mM MESNA and 1 mM tris(2-carboxyethyl) phosphine (TCEP). The columns were incubated at 4°C overnight after which the proteins were eluted with 2 bed volumes of CB. The eluates were analyzed on a 15% SDS–PAGE gel to investigate the IPL-mediated cleavage efficiency, and were either dialyzed overnight against phosphate-buffered saline (PBS, 137 mM NaCl, 2.7 mM KCl, 10 mM Na_2HPO_4 and 2 mM KH_2PO_4 at pH 7.4) using the Spectra/Por® 1 dialysis tubings (*MWCO* 6000–8000, Serva Electrophoresis), or immediately desalted and buffer-exchanged with PBS using the Amicon® Ultra concentrator (*MWCO* 3000, Merck Millipore). All buffers were filtered through a 0.22 mM membrane and aerated with nitrogen gas before use. All the protein concentrations were determined using the BCA protein assay kit for yield calculation, and the resulting protein solutions were stored at −20°C until further use.

Cytoplasmic expressions in *E.coli* SHuffle® T7 and nutrient-rich media

The production yields of nanobodies in *E.coli* SHuffle® T7 and in nutrient-rich media like TB and EnPresso® (all supplemented with the same amount of ampicillin as for LB) were investigated and compared with the expression using *E.coli* BL21(*DE3*) in LB. On the one hand, the cytoplasmic expressions of the constructs **5–7** were hereto performed using the two *E.coli* strains in LB as described above. On the other hand, the expression of construct **7** using *E.coli* SHuffle® T7 strain in TB was carried out as for LB (with the exception that the expression was performed at 28°C for 16 h after IPTG induction), whereas the culture in the EnPresso® was prepared as specified by the manufacturer as follows: the medium tablets were dissolved in sterile MilliQ water, then 1/2000 of Reagent A and the bacterial pre-culture were added for growth at 30°C overnight. On the next day, the IPTG (0.5 mM), Reagent A (1/2000) and the booster tablet were added and the expression was performed for another 24 h. For all experiments, cells were harvested by centrifugation and subjected to cytoplasmic extraction and subsequent IPL-mediated alkynation as described above.

Reduction with 2-mercaptoethylamine

The dialyzed NbVCAM1-LEY-alkyne and NbVCAM1-His_6-alkyne nanobodies (2–3 mg, concentrated to 1 mg/ml using the Amicon® Ultra concentrator) were reduced by adding a 180-fold molar excess of 2-mercaptoethylamine (2-MEA) as described by Massa *et al.* (2014).

Electrospray ionization-Fourier transform mass spectrometry

The dialyzed or desalted nanobodies and the nanobody-biotin conjugate (20 µM) were subjected to HPLC-MS to confirm their masses. Using a Dionex 3000 HPLC and auto-injector configuration, 30 µl aliquots of protein solutions were trapped and desalted for 5 min on a Dionex Acclaim PolarAdvantage II C18 reversed-phase 2.0 × 10 mm guard column (particle diameter 5 µm, porosity 120 Å) at a flow rate of 0.5 ml min^{-1} using 0.1% (v/v) formic acid in Milli-Q water (solvent A) directed to waste. Upon valve switching, elution was started for 7 min pumping 50% (v/v) acetonitrile in solvent A at a reduced flow rate of 0.1 ml min^{-1} into an electrospray ionization source with heated

auxiliary gas (5 arbitrary flow rate units; 55°C). Source voltage and capillary temperature were +4 kV and 275°C, respectively. The Orbitrap Velos Pro FTMS (Thermo Scientific) controlled by Thermo Xcalibur software v2.2 was operated in full scan mode in the mass range of 110–2000 Thomson at a resolution of 3×10^4 full width at half maximum with automatic gain control set to 1×10^6 ions in maximal 100 ms, without microscan averaging. Scans recorded between elution time 4 and 7 min were averaged. For molecular weight determination, the average spectrum was deconvoluted using Promass software for Xcalibur v2.8 (Novatia LLC). The deconvoluted masses were then compared with the theoretical values which were determined using CLC Main Workbench 6 software. Horse heart cytochrome C (8 µM in solvent A) was infused by a syringe pump at 5 µl min^{-1} as a tuning and calibration standard (average molecular mass of 12 360 Da).

Enzyme-linked immuno-sorbant assay

To determine the antigen-binding capacity of the different nanobody variants towards recombinant human VCAM1 (hVCAM1), the nanobodies were subjected to a sandwich enzyme-linked immuno-sorbant assay (ELISA). The NbVCAM1-His_6 and NbBcII-10-His_6 were used as positive and negative controls, respectively. A 96-well microplate was coated with 200 µl of a 5 µM nanobody solution in 0.1 M $NaHCO_3$ pH 8.2. After incubation overnight at 4°C, the plate was washed five times with Tris-buffered saline pH 8.0 (TBS) containing 0.5% (v/v) Tween 20 (TBST), blocked with 200 µl of 5% (w/v) skim milk powder in TBST at room temperature for 2 h and washed again five times with TBST. To each well, 100 µl of recombinant hVCAM1 in TBST was added in a concentration range of 0–100 ng/ml. The plate was incubated at room temperature for 5 h before washing five times with TBST. The captured antigen was incubated with 100 µl of 1 µg/ml mouse monoclonal anti-human IgG-alkaline phosphatase antibody (in TBST) at room temperature for 2 h, followed by washing three times with TBST. Subsequently, 200 µl of *p*-nitrophenyl phosphate substrate was added to each well and the plate was incubated at 37°C for 30 min before adding 50 µl of 3 M NaOH to stop the reaction. The plate was read immediately with a FLUOStar Omega Reader (BMG Labtech) to measure the absorbance at 405 nm (OD_{405}). All measurements were performed in triplicate and the data were processed with Graphpad Prism 5.0 software for statistical analysis.

CuAAC 'click' reaction with an azido-biotin derivative

The 'click' reactions were carried out in 200 µl PBS containing 10 µM purified nanobody, 0.2 mM azido-biotin, 1 mM TCEP, 0.1 mM tris-(benzyltriazolylmethyl)amine (TBTA) and 1 mM $CuSO_4$ (Crump *et al.*, 2011; Takamitsu *et al.*, 2014). The 'click' reaction was performed at room temperature under shaking for 2 h. The biotinylated product was analyzed by western blotting as follows: after analysis on a 15% SDS–PAGE gel, the proteins were transferred to an Amersham Hybond™-LFP Polyvinylidene fluoride (PVDF) membrane. The blot was blocked with 5% BSA for 1.5 h to inhibit non-specific binding. The biotinylated protein was incubated with streptavidin-alkaline phosphatase conjugate for 1 h and visualized by incubation with nitro blue tetrazolium chloride/5-bromo-4-chloro-3-indolyl phosphate substrate.

Results and discussion

Functional nanobodies can be produced in *E.coli* due to their much simpler structures when compared with conventional antibodies (Arbabi-Ghahroudi *et al.*, 2005; Baral and Arbabi-Ghahroudi, 2012), and mostly via periplasmic expression. For instance, this strategy was previously performed for the NbVCAM1-His_6 and the NbBcII-10-His_6 (Saerens *et al.*, 2004), as well as for other nanobodies targeting lysozyme epitope (Arbabi-Ghahroudi *et al.*, 1997), RNAse (Decanniere *et al.*, 1999), gelsolin (Van den Abbeele *et al.*, 2010) and human epidermal growth factor receptor 2 (EGFR) (Vaneycken *et al.*, 2011). In this study, the NbVCAM1-His_6 and NbBcII-10-His_6 (Fig. 1A) were successfully expressed in the periplasm in yields comparable with those described in the literature. Reulen *et al.* (2009) reported a periplasmic expression of the nanobody (sdAb-aGST)–intein–CBD fusion protein in *E.coli* using the *pelB* leader sequence. Their findings motivated our first attempts to obtain the NbVCAM1–intein–CBD fusion protein via such periplasmic expression strategy (Fig. 1B). However, due to its heterologous and chimeric nature, the *pelB*-mediated translocation of the large fusion protein to the periplasm might be inefficient. Therefore, we simultaneously explored the cytoplasmic expression of the fusion protein (Fig. 1C). Initially, the influence of various conditions such as the IPTG concentration, the incubation temperature and time on the expression level of the fusion protein was explored on a small scale.

Optimization of the NbVCAM1–intein–CBD expression

Fig. 2 shows SDS–PAGE profiles of the TCP content resulting from the periplasmic (construct **3**) and cytoplasmic (construct **4**) expression of the NbVCAM1–intein–CBD fusion protein using different IPTG concentrations and post-induction temperatures. The fusion protein with a molecular weight of ~42 kDa is clearly observed for the induced

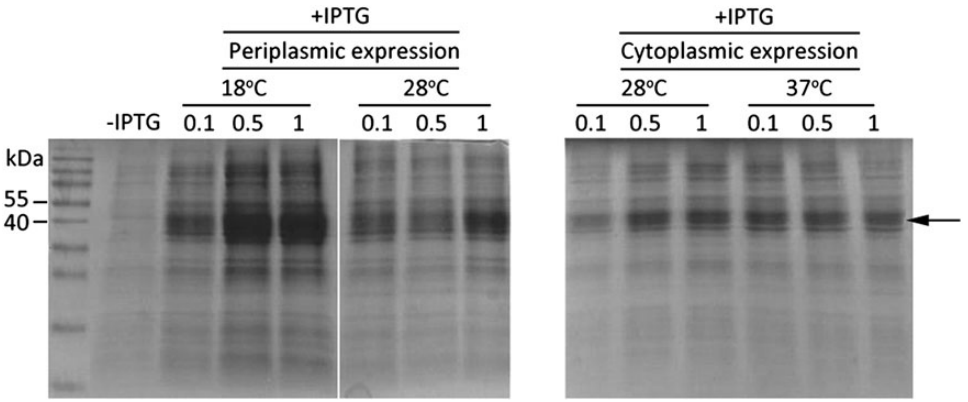

Fig. 2 TCP contents of *E.coli* BL21(*DE3*) cells grown and induced under different conditions to express the NbVCAM1–intein–CBD fusion protein (42 kDa, arrow). Post-induction periplasmic (left) and cytoplasmic (right) expressions were performed overnight and for 3 h, respectively.

cells. IPTG concentrations of 0.5 and 1 mM yield similar expression levels. However, for periplasmic expression (Fig. 2, left), an overnight expression at 18°C resulted in a higher amount of fusion protein when compared with an expression at 28°C. These low-temperature inductions generally slow down the protein production rate—which can be compensated for by a prolonged induction time—and might help decrease protein aggregation, which is crucial for an efficient export to the periplasm (Rosano and Ceccarelli, 2014). Cytoplasmic expression, on the other hand, can be performed at higher temperatures and shorter expression times (3 h). It is shown that the expression at 28 and 37°C resulted in a similar expression level (Fig. 2, right). Thus, for cytoplasmic expression, this means that the cells can be precultured and induced with IPTG for 3 h at 37°C without the need for a temperature change.

Expression of the fusion protein using *E.coli* BL21(*DE3*) in LB medium followed by IPL-mediated alkynation

At first instance, a large-scale periplasmic expression of the fusion protein from construct **3** was performed in *E.coli* BL21(*DE3*) using the optimized conditions described above (0.5 mM IPTG induction and overnight expression at 18°C). Despite the potential advantages of a periplasmic extraction, only a small amount of the fusion protein could be extracted from the periplasmic space by osmotic shock and most of the protein fraction remained in the cell debris (Fig. 3A). This is in contrast to the report of Reulen *et al.* (2009) who obtained a much larger amount of the sdAb-aGST-intein-fusion protein in the cell lysate. Our results suggest that (i) an improper folding of the NbVCAM1–intein–CBD fusion protein leads to an adverse influence on the *pelB*-mediated translocation to the periplasm, (ii) the *pelB* leader sequence did not function properly during protein processing and translocation or (iii) the fusion protein was stuck in the membrane due to an overload of the bacterial secretory machinery.

Extraction of the cytoplasmically expressed proteins, on the other hand, could be done easily with the B-PER reagent in a short time without additional physical aid from ultra-sonication or high-pressure shearing. Figure 3B shows that the majority of the protein from the cell lysate is soluble and thus the fusion protein can be captured on a chitin column. On-column cleavage of the nanobody from the intein–CBD fusion by either DTT or MESNA/TCEP/cysteine-alkyne linker was however unsuccessful as most of the fusion protein remained on the chitin resin (Fig. 3C). Most probably, this is due to the presence of an unfavorable C-terminal serine residue adjacent to the intein, resulting in a very low intein-mediated splicing efficiency (Xu and Evans, 2001). Therefore, the nanobodies were engineered with linker peptides to (i) create a space between the nanobody and the intein to facilitate proper folding of both proteins and (ii) to enhance the efficiency of the IPL-mediated cleavage by adding an amino acid that is favored by intein for the cleavage.

Tyrosine and histidine residues are reported to result in very high cleaving efficiencies of the proteins from the intein–CBD fusion part (Xu and Evans, 2001). Therefore, the C-terminus of the nanobody was either extended with five (EFLEY) or three (LEY) vector-derived amino acid residues, or with a His_6-tag. Since the spatial structure predictions of nanobodies engineered with these linkers (using the Phyre2 protein fold recognition engine (Kelley and Sternberg, 2009); data not shown) show no significant influence on the conformation of the NbVCAM1, it can be assumed that their binding capacities remain unchanged when compared with the wild-type nanobody (confirmed later by ELISA). Our results indeed showed that all three spacer peptides resulted in an almost 100% cleaving efficiency (based on SDS–PAGE results) of the nanobody with DTT or MESNA/TCEP/cysteine alkyne (Fig. 4). Only a small amount of self-cleavage (by hydrolysis) of the NbVCAM1-EFLEY was observed upon eluting with pure CB in the control experiment (Fig. 4A, lower panel). All proteins were obtained with high purity. The yields of the alkynated nanobodies obtained via cytoplasmic expression and IPL were 10–16 mg/l of *E.coli* culture using the BL21(*DE3*) strain in LB (Fig. 5A). This is about two to three times higher than the reported yield for the sdAb-aGST obtained via periplasmic expression (Reulen *et al.*, 2009). This is comparable with periplasmic yields of nanobodies reported in the literature, ranging from 0.8 to 10.5 mg for the NbVCAM1-His_6 (Broisat *et al.*, 2012) and 5 mg for the NbBCII-10-His_6 (Saerens *et al.*, 2005). Note that these two reference nanobodies were expressed in our study with comparable and even slightly higher yield (10.3 and 8.9 mg/l of *E.coli* culture for NbVCAM1-His_6 and NbBCII-10-His_6, respectively; see Fig. 1). Although the alkynated nanobodies were obtained in good yields, we decided to perform the cytoplasmic expression protocol using the *E.coli* SHuffle® T7 strain and nutrient-rich growth media in order to further improve the yield.

Influence of *E.coli* SHuffle® T7 strain and nutrient-rich media on the alkynated nanobody yield

The expression of the three nanobodies with different spacer peptides under the optimized conditions as described above was repeated in the *E.coli* SHuffle® T7 strain and compared with the yields obtained by using the BL21(*DE3*) strain. The *E.coli* SHuffle® T7 strain co-expresses the DsbC chaperone to correct for misformation of disulfide bonds and to promote proper protein folding (de Marco, 2012). This

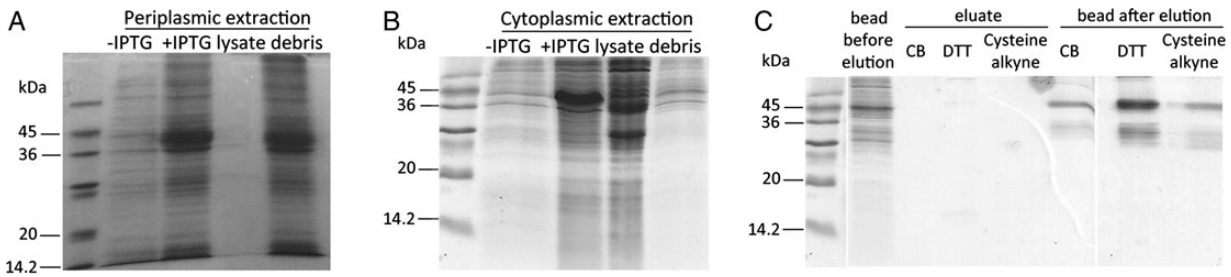

Fig. 3 SDS–PAGE analysis of the of NbVCAM1–intein–CBD fusion proteins resulting from cell extractions obtained from (**A**) periplasmic and (**B**) cytoplasmic expressions. The TCP content of the non-induced and IPTG-induced cells as well as the cell lysate and cell debris was resolved on the gels. (**C**) SDS–PAGE profile of all fractions from the IPL-mediated purification process of the cell lysate obtained from the cytoplasmic expression. The NbVCAM1–intein–CBD fusion protein was captured on the chitin beads and the cleavage of the nanobody was performed using pure CB, CB containing DTT or CB containing TCEP/MESNA/cysteine alkyne (depicted as CB, DTT and Cysteine alkyne, respectively).

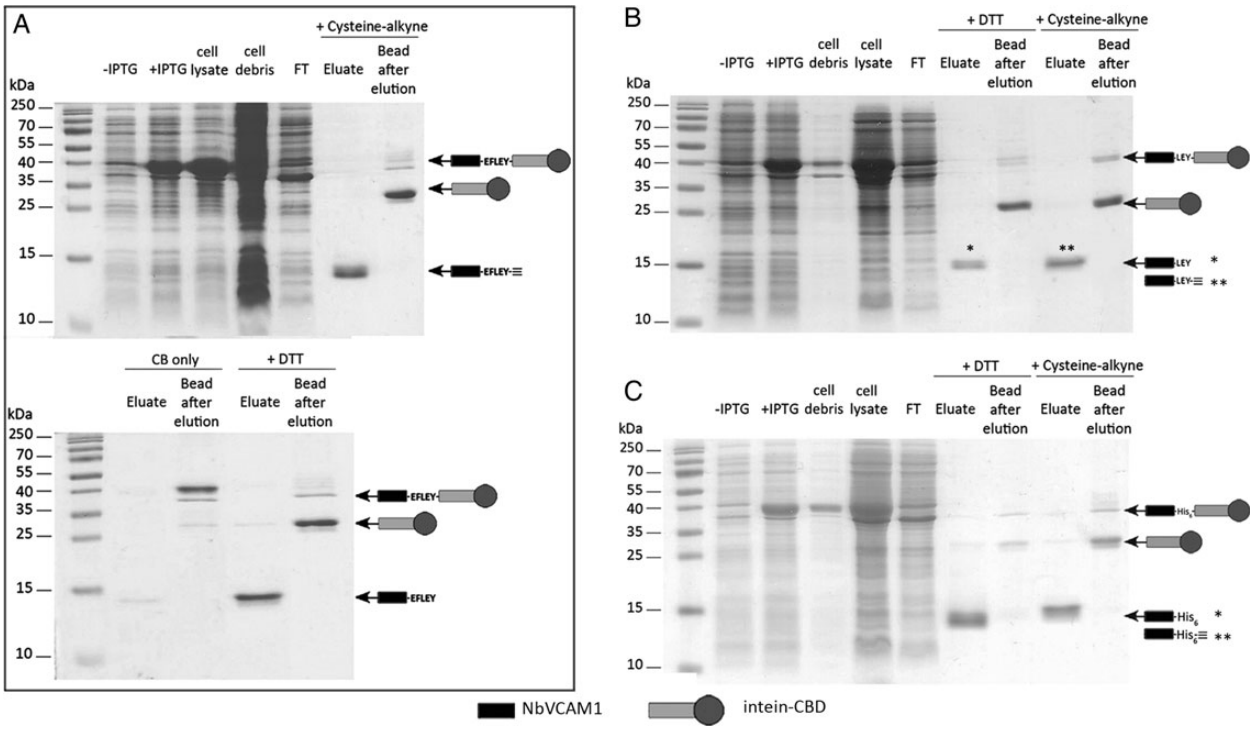

Fig. 4 SDS–PAGE profiles of all fractions from the IPL-mediated purification process of different nanobody variants on a chitin column: (**A**) NbVCAM1-EFLEY (upper and lower panel), (**B**) NbVCAM1-LEY and (**C**) NbVCAM1-His_6 obtained from the corresponding cytoplasmically expressed fusion proteins via the same protocol as described for Fig. 3C. The samples loaded on the gel are TCP contents of the non-induced and IPTG-induced cells, the cell lysate, the cell debris, flow through (FT), eluate, chitin beads after IPL-mediated cleavage and elution. On the right of the gels, illustrative protein structures of the corresponding fractions are presented.

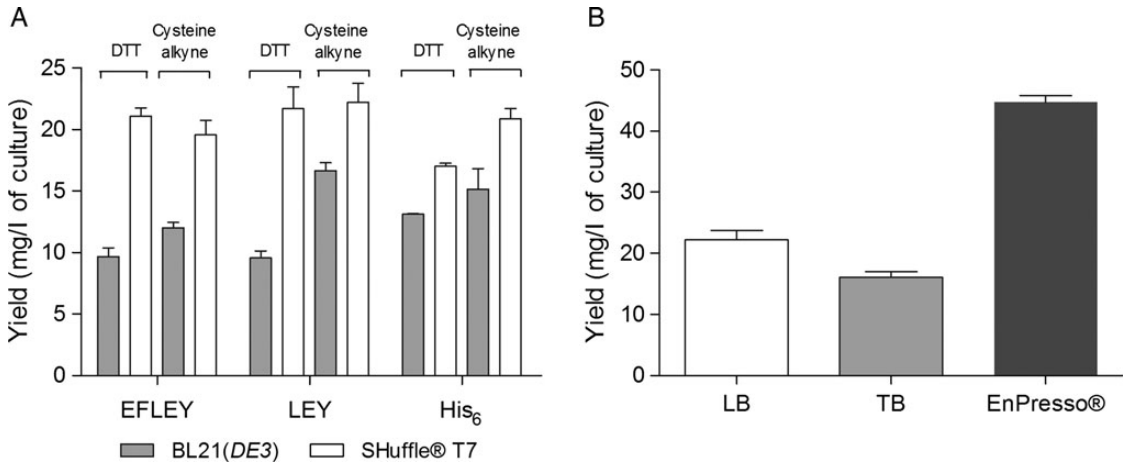

Fig. 5 Expression yields of the nanobodies engineered with different C-terminal spacer peptides in two different *E.coli* strains. The nanobodies were cleaved from the intein with CB containing DTT or CB containing MESNA/TCEP/cysteine alkyne (represented as DTT and Cysteine alkyne, respectively, on top of the graph) (**A**). Expression yield of the alkynated nanobody (NbVCAM1-LEY-alkyne) in the SHuffle® T7 *E.coli* strain using different media (**B**). All cultures were grown in triplicate and the reported values correspond to the averages with their standard deviations.

is important to obtain more soluble fusion protein, and consequently more alkynated nanobodies via IPL. The NbVCAM1 itself contains only two cysteine residues, so only one thiol combination and one disulfide bond is possible. The DsbC isomerase is able to protect this intradomain disulfide bond from the reducing cytoplasmic environment during expression by re-oxidizing the bond to form the functional structure again. As can be observed in Fig. 5A, all nanobody variants were expressed in significantly higher yield in the SHuffle® T7 strain. The alkynated NbVCAM1-EFLEY, NbVCAM1-LEY and NbVCAM1-His_6 were expressed at 19.6, 22.2 and 20.9 mg/l of *E.coli* culture, respectively.

As mentioned earlier, since the three spacer peptides assumptively have no influence on the nanobody's structure, it can also be hypothesized that the folding and hence expression yield of the NbVCAM1-EFLEY-alkyne and NbVCAM1-His_6-alkyne would be rather similar to this of the NbVCAM1-LEY-alkyne when using the same media

and the same *E.coli* strain. Therefore, only the NbVCAM1-LEY-alkyne was further investigated with respect to its expression in nutrient-rich media (TB and EnPresso®), by using the SHuffle® T7 *E.coli* strain, in comparison to the conventional LB medium. Our result showed that using the TB medium, the yield was lower than in the LB medium (Fig. 5B), which is in contrast to the findings of Zarschler *et al.* (2013), who reported a better expression yield in TB. This is probably due to the long expression period (16 h), which might result in protein aggregation and/or proteolytic degradation. On the other hand, the use of EnPresso® medium resulted in a doubling of the yield (Fig. 5B). This 2-fold increase in yield is, however, lower than the 5-fold increase as reported by Zarschler *et al.* (2013) for the expression of the single-domain antibody against the HER in EnPresso® medium when compared with the LB medium. This result can be explained by the fact that the synthesis and folding of the single-domain antibody take place much faster and more efficiently when compared with the chimeric nanobody–intein–CBD protein. Taking the relatively high cost and time-consuming expression process (2 days) of the EnPresso® medium into account, the proposed expression protocol (LB medium—SHuffle® T7 *E.coli* strain—cytoplasmic expression) is faster (3 h) and cheaper.

Although previous studies reported the IPL-mediated alkynation as a useful tool to produce alkynated nanobodies for CuAAC-mediated click couplings, the documented yields are rather low. The yields obtained in this study via cytoplasmic expression in *E.coli* SHuffle® T7 and LB medium are ~4–10 times higher than the reported yield for the periplasmic expression of sdAb-aGST, which was 2–5 mg/l of culture using the classical BL21(*DE3*) *E.coli* strain (Reulen *et al.*, 2009). Expression of a nanobody in the cytoplasm of *E.coli* has been reported for the PlexinD1-targeting nanobody but no yields were reported unfortunately (Debets *et al.*, 2013a,b). Besides the cytoplasmic expression in SHuffle® T7 strain, this major difference can also be attributed to the engineering of the nanobodies with the spacer peptides. To the best of our knowledge, no other paper reports on a progress in yield of this order for alkynated nanobodies, and more general for any C-terminal modification of nanobodies. Without doubt, it opens a way towards an upscaling for the preparation of functionalized nanobodies needed to explore innovative applications.

Structural characterization of the modified nanobody variants by mass spectrometry

All purified nanobodies were analyzed by electrospray ionization-Fourier transform mass spectrometry (ESI-FTMS) for quality control (purity and degree of alkynation at the C-terminus). An overview of all theoretical and experimental masses of relevant nanobodies is given in Supplementary Table S3. In the deconvoluted spectrum of NbVCAM1-EFLEY (elution with DTT, Fig. 6A), two masses are observed (14648.8 and 14784.4 Da) of which the former represents the theoretical mass (14650.18 Da) of the non-alkynated NbVCAM1-EFLEY nanobody. The latter, with a mass increase of ~135 Da, results from the DTT-nanobody precursor from which the DTT is not completely removed by hydrolysis. This agrees with the findings of Chong *et al.* (1997), who reported a mixture of wild-type and DTT-conjugated MBP after IPL. Similar findings were observed for NbVCAM1-LEY (eluted with DTT) with the detection of masses of 14372.9 and 14507.9 Da (Fig. 6C).

In the mass spectrum of the NbVCAM1-EFLEY-alkyne fraction (eluted with MESNA/cysteine alkyne, Fig. 6B), a major peak representing a mass of 14929 Da was detected, i.e. corresponding to a mass increase of ~280 Da when compared with the unmodified protein (14648.8 Da). This mass increase is consistent with the attachment of a cysteine-alkyne linker (158 Da) to which an additional MESNA molecule (142 Da) is coupled via a disulfide bond. In more detail, the linker molecule is bonded to the C-terminus via a peptide bond (condensation reaction with the loss of H_2O—thus causing a mass increase of only 140 Da) and the formation of the disulfide bond with MESNA, causing a second mass increase of 140 Da. The mass of such a MESNA-conjugated alkynated nanobody is also the major one observed in the mass spectra of the NbVCAM1-LEY-alkyne (eluted with TCEP/MESNA/cysteine alkyne, Fig. 6D) and the NbVCAM1-His_6-alkyne (eluted with TCEP/MESNA/cysteine alkyne, Fig. 6E). For the NbVCAM1-LEY-alkyne (Fig. 6D) also the mono-alkynated nanobody without MESNA is significantly present.

More in general, due to the presence of the free thiol on the C-terminally coupled cysteine-alkyne linker, disulfide pairing with another free thiol group (arising from MESNA, a second cysteine-alkyne linker or another mono-alkynated nanobody) can occur for the mono-alkynated nanobody during IPL and dialysis. This possibly results in unwanted nanobody variants, i.e. (i) MESNA-conjugated mono-alkynated nanobody (as seen in Fig. 6B, D and E), (ii) bi-alkynated nanobody (very unlikely since the concentration of MESNA is in large excess with respect to the cysteine-alkyne linker) and (iii) the dimeric form of the mono-alkynated nanobodies. These unwanted, additionally coupled molecules can be decoupled from the mono-alkynated nanobodies by reducing the disulfide bond between them. The released MESNA and cysteine-alkyne linker could be removed via desalting afterwards, resulting in purely mono-alkynated nanobodies. In order to reduce these additional disulfide bonds without interfering with the essential intradomain disulfide bond, the mild reducing reagent 2-MEA was added to the dialyzed nanobodies, according to Massa *et al.* (2014). As seen from the mass spectra of such reduced samples (Supplementary Fig. S2 for NbVCAM1-LEY-alkyne and NbVCAM1-His_6-alkyne), ~50% of the nanobody population consists of the mono-alkynated nanobody while the other 50% has 2-MEA coupled via a disulfide bond (instead of MESNA before reduction with 2-MEA). Comparing to the mass spectra of the non-reduced samples (Fig. 6D and E), more than half of the MESNA-conjugated NbVCAM1-His_6-alkyne could be reduced to NbVCAM1-His_6-alkyne, whereas the use of 2-MEA was less effective for the MESNA-conjugated NbVCAM1-LEY-alkyne. Alternatively, instead of using 2-MEA, the NbVCAM1-LEY-alkyne fraction eluted from the chitin column after IPL was immediately desalted and buffer-exchanged with nitrogen-aerated PBS buffer in order to avoid the long dialysis time during which the unwanted oxidative couplings (as described above) seem to take place (note that the concentration of the reducing reagent TCEP decreases during dialysis). The mass spectrum of the desalted NbVCAM1-LEY-alkyne (Fig. 6F) confirms this by representing only the mass of the purely mono-alkynated species (14 512 Da). This observation clearly demonstrates that immediate desalting and buffer exchanging with N_2-aerated buffer is very effective to avoid oxidative couplings in general.

All by all, the above results describe an efficiency of almost 100% for the IPL-mediated C-terminal alkynation of the nanobodies by using our proposed protocol. This is in contrast to a reported efficiency of only 50% for the nanobody against PlexinD1 (Debets *et al.*, 2013a,b). It indicates that our protocol opens the door towards large-scale and high-throughput production of mono-alkynated nanobodies.

Nanobody functionality and clickability

The alkynated nanobodies were tested for their antigen-binding capacity in order to look for the influence of cytoplasmic expression

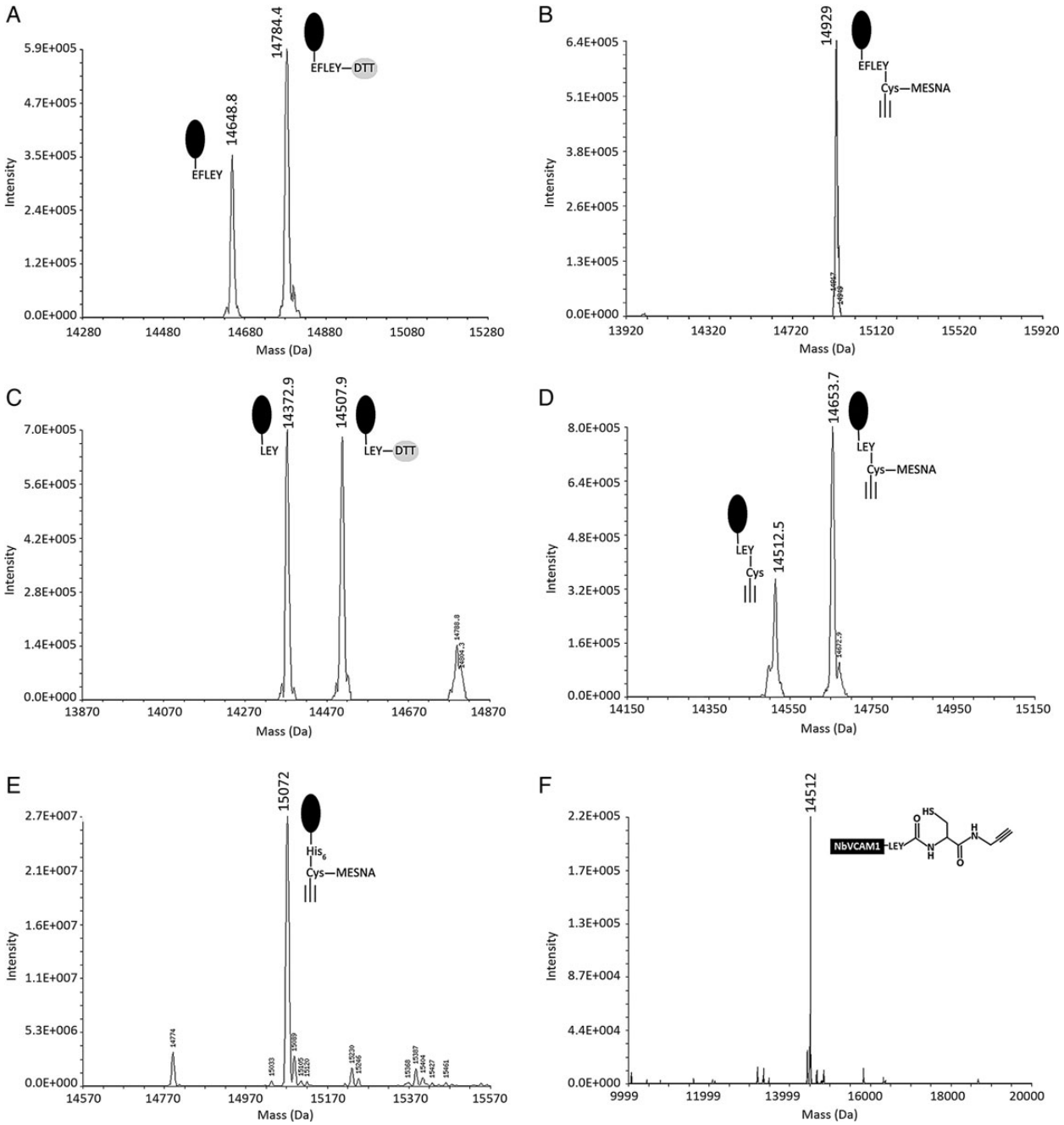

Fig. 6 ESI-FTMS spectra of the NbVCAM1-EFLEY fraction obtained after cleavage with DTT (**A**) or TCEP/MESNA/cysteine alkyne (**B**), showing two masses corresponding to non-alkynated NbVCAM1-EFLEY and NbVCAM1-EFLEY-DTT (A), and only the MESNA-conjugated alkynated NbVCAM1-EFLEY (B). A similar mass spectrum was obtained for the unalkynated NbVCAM1-LEY and NbVCAM1-LEY-DTT (**C**), whereas both mono-alkynated NbVCAM1-LEY and MESNA-conjugated alkynated NbVCAM1-LEY were observed in (**D**). The mass spectrum of the His_6-tagged nanobody resulting from IPL-mediated cleavage with MESNA/TCEP/cysteine alkyne mainly shows the MESNA-conjugated alkynated nanobodoy (**E**). The mass spectrum of desalted and buffer-exchanged NbVCAM1-LEY-alkyne (using amicon concentrator with N_2-aerated PBS buffer) showing quasi only mono-alkynated NbVCAM1-LEY-alkyne (**F**). Representative structures of the corresponding nanobody species are displayed next to the corresponding mass peaks.

and IPL on the protein functionality. Hereto, the recombinant human VCAM1 antigen was detected in a broad concentration range by means of a sandwich ELISA. As demonstrated in Fig. 7A, all NbVCAM1 variants still have a similar binding capacity as the reference NbVCAM1-His_6, indicating that the cytoplasmic expression, the *in vitro* IPL, as well as the MESNA-conjugation or dimerization of mono-alkynated nanobodies (if present) have no impact on the nanobody activity. Moreover, the C-terminal alkyne functions remain accessible even if the MESNA-conjugation or self-dimerization of the nanobody occurs. However, this unwanted conjugation/dimerization can be avoided by quickly desalting and buffer exchanging as described above, leading to an excellent homogeneity of C-terminally mono-alkynated nanobodies. This can become an important advantage in the race towards highly homogenous couplings to other molecules or surfaces, which is of high concern in bioconjugation.

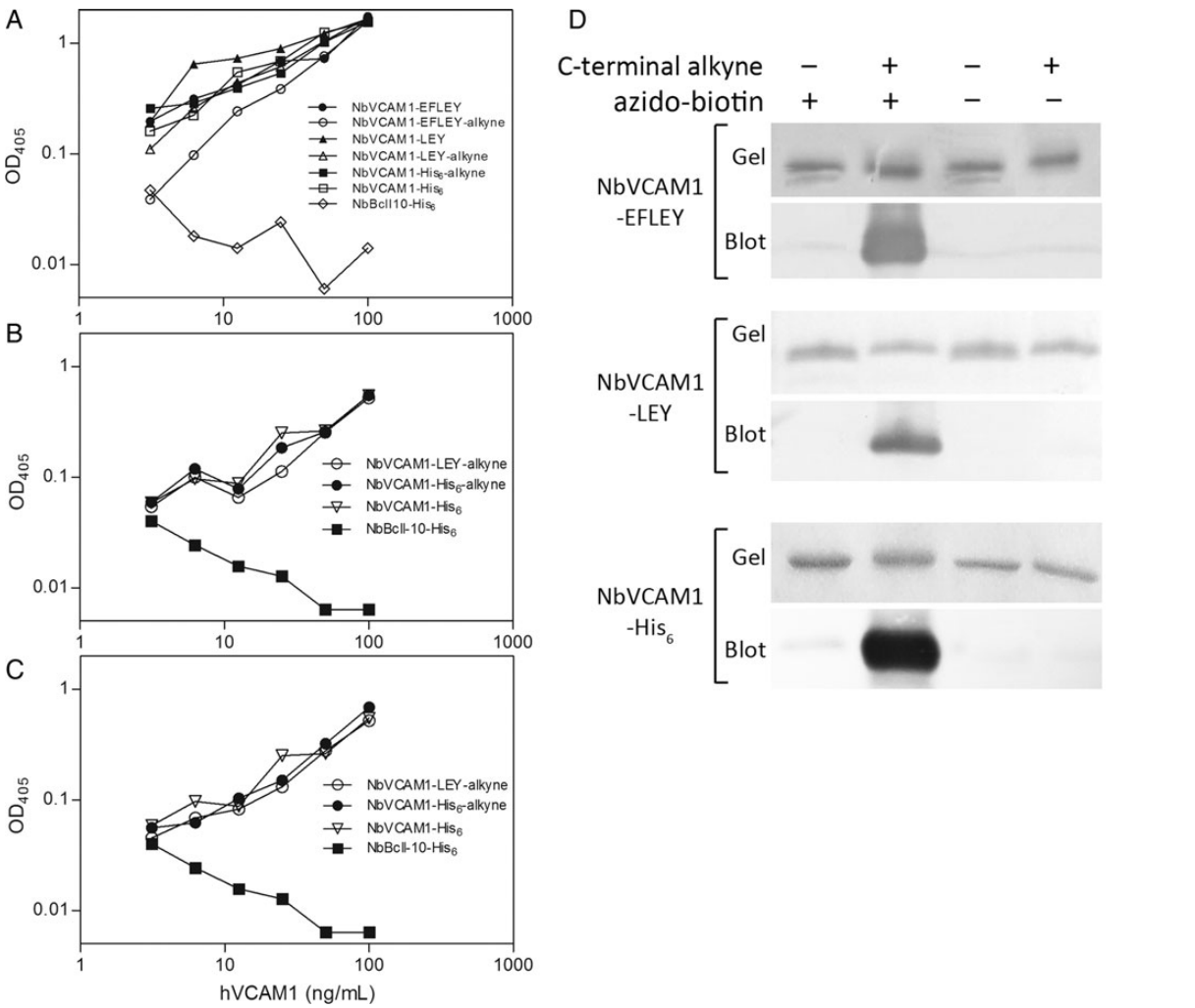

Fig. 7 Sandwich ELISA results, showing the binding capacity of the nanobody variants towards the recombinant human VCAM1: (**A**) the nanobody variants purified as described in the caption of Fig. 4. (**B**) The unreduced and (**C**) 2-MEA reduced NbVCAM1-LEY-alkyne and NbVCAM1-His_6-alkyne fractions. The periplasmically expressed NbVCAM1-His_6 and NbBcII-10-His_6 were used as positive and negative controls, respectively. (**D**) SDS–PAGE and western blots of CuAAC-mediated biotinylation of the nanobodies. The 'click' reactions were performed for unmodified and C-terminally alkynated nanobodies in the presence or absence of the azido-biotin derivative.

Although the *E.coli* SHuffle® T7 strain was able to protect the nanobodies from cytoplasmic reduction, the *in vitro* modification via IPL makes use of several reducing reagents such as DTT, MESNA, TCEP and cysteine alkyne. It was therefore concerned if these reagents could have an influence on the spatial structure and function since the nanobodies contain an essential intradomain disulfide bond connecting the two CDR domains. If this intradomain disulfide bond would have been reduced, the nanobody could become conjugated with one or more of these reducing molecules, resulting in complicated mass spectra. As this situation is clearly not observed, the concentration/reducing power of these reducing reagents can be considered as mild with respect to the nanobody's structure and functionality. This is furthermore confirmed by the unchanged activity of the nanobodies after reduction with 2-MEA as demonstrated by ELISA in Fig. 7B and C.

All alkynated nanobody variants could be coupled to the azido-biotin derivative through CuAAC chemistry, as a confirmation of the clickability of their introduced alkyne functions (Fig. 7D), while this was impossible for the non-alkynated nanobodies. The ESI-FTMS spectrum (Fig. 8) shows that, even without optimization of the reaction conditions reported

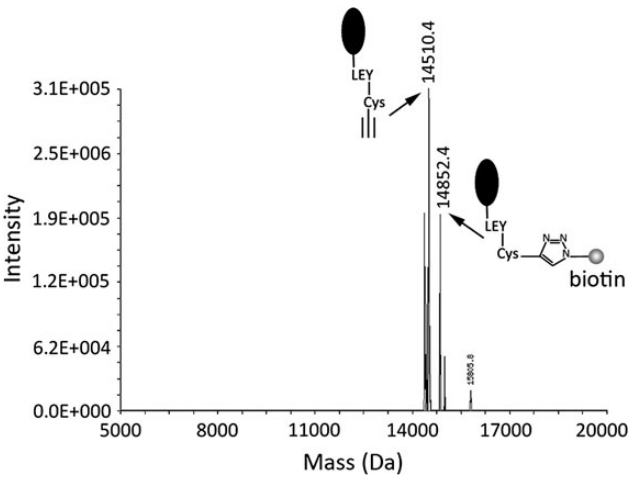

Fig. 8 ESI-FTMS spectrum of the biotin-conjugated NbVCAM1-LEY-alkyne.

in the literature, the conjugation of NbVCAM1-LEY-alkyne with azido-biotin could be achieved with a yield of ~40%. This is in agreement with a study of Besanceney-Webler *et al.* (2011) who reported that the use of TBTA results in a kinetically slow coupling reaction. This also indicates that the alkyne function is accessible for the CuAAC-mediated coupling reaction, and that the bioorthogonal C-terminal alkynation does not interfere with the functional conformation of the nanobodies. Although all three alkynated nanobodies with spacer peptides could be obtained in high yields and retained good binding capacity, the achieved results suggest a slightly prominence of the alkynated NbVCAM1-LEY and NbVCAM1-EFLEY due to their higher alkynation degrees. Besides, engineering of the LEY spacer peptide also causes less mutation in the nanobody (compared with the EFLEY), and consequently less expected variation in performance when compared with the wild-type nanobody. All the above results indicate the robustness of our proposed expression and IPL protocol for nanobodies, not only towards an efficient bioorthogonal and site-specific alkynation but also for their subsequent covalent and uniformly oriented coupling to various innovative azide-containing substances. It can also be expected that the proposed protocol will be applicable to other bioorthogonal, site-specific nanobody modifications (e.g. Diels-Alder couplings) too.

Conclusions

The VCAM1-targeting nanobody (NbVCAM1) was engineered towards the site-specific incorporation of a bioorthogonal alkyne function at its C-terminus via the IPL technique. The nanobody was most efficiently expressed as a NbVCAM1-LEY–intein–CBD fusion protein in the cytoplasm of *E.coli* SHuffle® T7 cells at 37°C during 3 h in LB medium, and subsequently C-terminally alkynated via IPL with a yield of around 22 mg/l and an alkynation efficiency of ~100%. To the best of our knowledge, this is the first time that such a progress in yield and degree of modification is reported for alkynated nanobodies. The resulting nanobody was obtained as a purely mono-alkynated variant and preserved the same antigen-binding capacity as the unmodified nanobody. Moreover, successful coupling to an azido-biotin derivative using CuAAC 'click' chemistry was demonstrated. Taking the well-known stability of nanobodies into account, the proposed protocol can be considered as a generic, highly productive synthesis method to append bioorthogonal functionalities to the C-terminus, paving the way towards innovative applications.

Supplementary data

Supplementary data are available at *PEDS* online.

Acknowledgements

We thank Prof. Dr Serge Muyldermans (VUB, Belgium) for kindly providing the vector pHEN6(c):*pelB*-Nb-VCAM1-His_6. We kindly acknowledge the financial support from the Hercules Foundation in the framework of the project 'LC-MS@UHasselt: Linear Trap Quadrupole-Orbitrap mass spectrometer' and thank Mr Erik Rooyackers for the MS measurements. We also want to thank the Interreg IV-A project 'BioMiMedics' (www.biomimedics.org) for the financial contribution from the EU and the province of Limburg-Belgium. We further acknowledge the financial support from the Interuniversity Attraction Poles Programme (P7/05) initiated by the Belgian Science Policy Office (BELSPO).

Funding

This work was funded by the Fund for Scientific Research of Flanders (FWO-Vlaanderen) via the project G.0581.12N.

References

Arbabi-Ghahroudi,M., Desmyter,A., Wyns,L., Hamers,R. and Muyldermans, S. (1997) *FEBS Lett.*, **414**, 521–526.
Arbabi-Ghahroudi,M., Tanha,J. and MacKenzie,R. (2005) *Cancer Metastasis Rev.*, **24**, 501–519.
Ayers,B., Blaschke,U.K., Camarero,J.A., Cotton,G.J., Holford,M. and Muir,T. W. (1999) *Biopolymers*, **51**, 343–354.
Baral,T.N. and Arbabi-Ghahroudi,M. (2012) *Methods Mol. Biol.*, **911**, 257–275.
Bell,A., Wang,Z.J. and Arbabi-Ghahroudi,M., , *et al.* (2010) *Cancer Lett.*, **289**, 81–90.
Besanceney-Webler,C., Jiang,H., Zheng,T., *et al.* (2011) *Angew. Chem. Int. Ed.*, **50**, 8051–8056.
Bessette,P.H., Aslund,F., Beckwith,J. and Georgiou,G. (1999) *Proc. Natl Acad. Sci. U.S.A.*, **96**, 13703–13708.
Best,M.D. (2009) *Biochemistry*, **48**, 6571–6584.
Broisat,A., Hernot,S. and Toczek,J., , *et al.* (2012) *Circ. Res.*, **110**, 927–937.
Carboni,B., Benalil,A. and Vaultier,M. (1993) *J. Org. Chem.*, **58**, 3736–3741.
Chakravarty,R., Goel,S. and Cai,W. (2014) *Theranostics*, **4**, 386–398.
Chen,J., Song,J.L., Zhang,S., Wang,Y., Cui,D.F. and Wang,C.C. (1999) *J. Biol. Chem.*, **274**, 19601–19605.
Choi,S.R., Seo,J.S., Bohaty,R.F. and Poulter,C.D. (2014) *Bioconjug. Chem.*, **25**, 269–275.
Chong,S., Mersha,F.B. and Comb,D.G., , *et al.* (1997) *Gene*, **192**, 271–281.
Corisdeo,S. and Wang,B. (2004) *Protein Expr. Purif.*, **34**, 270–279.
Crump,C.J., Fish,B.A., Castro,S.V., *et al.* (2011) *ACS Chem. Neurosci.*, **2**, 705–710.
Dawson,P.E., Muir,T.W., Clark-Lewis,I. and Kent,S.B. (1994) *Science*, **266**, 776–779.
Dean,K.M. and Palmer,A.E. (2014) *Nat. Chem. Biol.*, **10**, 512–523.
Debets,M.F., van Berkel,S.S., Dommerholt,J., Dirks,A.T., Rutjes,F.P. and van Delft,F.L. (2011) *Acc. Chem. Res.*, **44**, 805–815.
Debets,M.F., Leenders,W.P., Verrijp,K., Zonjee,M., Meeuwissen,S.A., Otte-Holler,I. and van Hest,J.C. (2013a) *Macromol. Biosci.*, **13**, 938–945.
Debets,M.F., van Hest,J.C. and Rutjes,F.P. (2013b) *Org. Biomol. Chem.*, **11**, 6439–6455.
Decanniere,K., Desmyter,A., Lauwereys,M., Ghahroudi,M.A., Muyldermans, S. and Wyns,L. (1999) *Structure*, **7**, 361–370.
De Genst,E., Saerens,D., Muyldermans,S. and Conrath,K. (2006) *Dev. Comp. Immunol.*, **30**, 187–198.
de Marco,A. (2012) *Microb. Cell Fact.*, **11**, 129.
Dennler,P., Chiotellis,A., Fischer,E., Bregeon,D., Belmant,C., Gauthier,L., Lhospice,F., Romagne,F. and Schibli,R. (2014) *Bioconjug. Chem.*, **25**, 569–578.
Dumoulin,M., Conrath,K., Van Meirhaeghe,A., Meersman,F., Heremans,K., Frenken,L.G., Muyldermans,S., Wyns,L. and Matagne,A. (2002) *Protein Sci.*, **11**, 500–515.
Ghassabeh,G., Saerens,D. and Muyldermans,S. (2010) In Kontermann,R. and Dübel,S. (eds), *Antibody Engineering*. Springer, Berlin, Heidelberg, pp. 251–266.
Ghosh,I., Considine,N., Maunus,E., Sun,L., Zhang,A., Buswell,J., Evans,T.C., Jr. and Xu,M.Q. (2011) *Methods Mol. Biol.*, **705**, 87–107.
Hao,Z., Hong,S., Chen,X. and Chen,P.R. (2011) *Acc. Chem. Res.*, **44**, 742–751.
Hapuarachchige,S., Zhu,W., Kato,Y. and Artemov,D. (2014) *Biomaterials*, **35**, 2346–2354.
Harmsen,M.M. and De Haard,H.J. (2007) *Appl. Microbiol. Biotechnol.*, **77**, 13–22.
Hassanzadeh-Ghassabeh,G., Saerens,D. and Muyldermans,S. (2011) *Methods Mol. Biol.*, **790**, 239–259.
Hassanzadeh-Ghassabeh,G., Devoogdt,N., De Pauw,P., Vincke,C. and Muyldermans,S. (2013) *Nanomedicine*, **8**, 1013–1026.
Heal,W.P., Jovanovic,B., Bessin,S., Wright,M.H., Magee,A.I. and Tate,E.W. (2011) *Chem. Commun. (Camb.)*, **47**, 4081–4083.
Herner,A., Estrada Girona,G., Nikic,I., Kallay,M., Lemke,E.A. and Kele,P. (2014) *Bioconjug. Chem*, **25**, 1370–1374.

Kelley,L.A. and Sternberg,M.J.E. (2009) *Nat. Protocols*, **4**, 363–371.
Kijanka,M., Dorresteijn,B., Oliveira,S. and van Bergen En Henegouwen,P.M. (2015) *Nanomedicine (Lond.)*, **10**, 161–174.
Lang,K., Davis,L., Torres-Kolbus,J., Chou,C., Deiters,A. and Chin,J.W. (2012) *Nat. Chem.*, **4**, 298–304.
Levy,R., Weiss,R., Chen,G., Iverson,B.L. and Georgiou,G. (2001) *Protein Expr. Purif.*, **23**, 338–347.
Lim,S.I., Mizuta,Y., Takasu,A., Kim,Y.H. and Kwon,I. (2014) *PLoS ONE*, **9**, e98403.
Lin,P.C., Ueng,S.H., Tseng,M.C., Ko,J.L., Huang,K.T., Yu,S.C., Adak,A.K., Chen,Y.J. and Lin,C.C. (2006) *Angew. Chem. Int. Ed. Engl.*, **45**, 4286–4290.
Luan,C., Xie,Y.G., Pu,Y.T., Zhang,H.W., Han,F.F., Feng,J. and Wang,Y.Z. (2014) *Can. J. Microbiol.*, **60**, 113–120.
Makrides,S.C. (1996) *Microbiol. Rev.*, **60**, 512–538.
Massa,S., Xavier,C., De Vos,J., Caveliers,V., Lahoutte,T., Muyldermans,S. and Devoogdt,N. (2014) *Bioconjug. Chem.*, **25**, 979–988.
Meldal,M. and Tornoe,C.W. (2008) *Chem. Rev.*, **108**, 2952–3015.
Muir,T.W., Dawson,P.E. and Kent,S.B. (1997) *Meth. Enzymol.*, **289**, 266–298.
Muir,T.W., Sondhi,D. and Cole,P.A. (1998) *Proc. Natl Acad. Sci. U.S.A.*, **95**, 6705–6710.
Muyldermans,S., Atarhouch,T., Saldanha,J., Barbosa,J.A. and Hamers,R. (1994) *Protein Eng.*, **7**, 1129–1135.
Muyldermans,S., Baral,T.N. and Retamozzo,V.C., , *et al.* (2009) *Vet. Immunol. Immunopathol.*, **128**, 178–183.
Naganathan,S., Ye,S., Sakmar,T.P. and Huber,T. (2013) *Biochemistry*, **52**, 1028–1036.
Nguyen,V., Conyers,J.M., Zhu,D., Gibo,D.M., Hantgan,R.R., Larson,S.M., Debinski,W. and Mintz,A. (2012) *Neuro-oncology*, **14**, 1239–1253.
O'Brien,K.D., Allen,M.D., McDonald,T.O., *et al.* (1993) *J. Clin. Invest.*, **92**, 945–951.
Reulen,S.W., van Baal,I., Raats,J.M. and Merkx,M. (2009) *BMC Biotechnol.*, **9**, 66.
Rodriguez Camargo,D.C., Tripsianes,K., Kapp,T.G., Mendes,J., Schubert,J., Cordes,B. and Reif,B. (2015) *Protein Expr. Purif.*, **106**, 49–56.
Rosano,G.L. and Ceccarelli,E.A. (2014) *Front. Microbiol.*, **5**, 172.
Saerens,D. (2010) *World J. Biol. Chem.*, **1**, 235–238.
Saerens,D., Kinne,J., Bosmans,E., Wernery,U., Muyldermans,S. and Conrath, K. (2004) *J. Biol. Chem.*, **279**, 51965–51972.
Saerens,D., Pellis,M., Loris,R., Pardon,E., Dumoulin,M., Matagne,A., Wyns, L., Muyldermans,S. and Conrath,K. (2005) *J. Mol. Biol.*, **352**, 597–607.
Schneider,D., Schneider,T., Rosner,D., Scheffner,M. and Marx,A. (2013) *Bioorg. Med. Chem.*, **21**, 3430–3435.
Shioi,K., Komiya,A. and Hattori,K., , *et al.* (2006) *Clin. Cancer Res.*, **12**, 7339–7346.
Steen Redeker,E., Ta,D.T., Cortens,D., Billen,B., Guedens,W. and Adriaensens, P. (2013) *Bioconjug. Chem.*, **24**, 1761–1777.
Steinhagen,M., Holland-Nell,K., Meldal,M. and Beck-Sickinger,A.G. (2011) *Chembiochem*, **12**, 2426–2430.
Takamitsu,E., Fukunaga,K., Iio,Y., Moriya,K. and Utsumi,T. (2014) *Anal. Biochem.*, **464**, 83–93.
Tarasava,K. and Freisinger,E. (2014) *Protein Eng. Des. Sel.*, **27**, 481–488.
Tornoe,C.W., Christensen,C. and Meldal,M. (2002) *J. Org. Chem.*, **67**, 3057–3064.
Touvier,M., Fezeu,L. and Ahluwalia,N., , *et al.* (2012) *World J. Gastroenterol.*, **18**, 2805–2812.
Trilling,A.K., Hesselink,T., van Houwelingen,A., Cordewener,J.H., Jongsma, M.A., Schoffelen,S., van Hest,J.C., Zuilhof,H. and Beekwilder,J. (2014) *Biosens. Bioelectron.*, **60**, 130–136.
Van den Abbeele,A., De Clercq,S., De Ganck,A., *et al.* (2010) *Cell. Mol. Life Sci.*, **67**, 1519–1535.
Vaneycken,I., Devoogdt,N., Van Gassen,N., Vincke,C., Xavier,C., Wernery,U., Muyldermans,S., Lahoutte,T. and Caveliers,V. (2011) *FASEB J.*, **25**, 2433–2446.
van Vught,R., Pieters,R.J. and Breukink,E. (2014) *Comput. Struct. Biotechnol. J.*, **9**, 13.
Warren,T.D., Coolbaugh,M.J. and Wood,D.W. (2013) *Protein Expr. Purif.*, **91**, 169–174.
Wood,D.W. and Camarero,J.A. (2014) *J. Biol. Chem.*, **289**, 14512–14519.
Xu,M.Q. and Evans,T.C., Jr. (2001) *Methods*, **24**, 257–277.
Zarschler,K., Witecy,S., Kapplusch,F., Foerster,C. and Stephan,H. (2013) *Microb. Cell Fact.*, **12**, 97.
Zeglis,B.M., Sevak,K.K., Reiner,T., Mohindra,P., Carlin,S.D., Zanzonico,P., Weissleder,R. and Lewis,J.S. (2013) *J. Nucl. Med.*, **54**, 1389–1396.